

Neuroprotective Effect of Combined Treatment with Epigallocatechin 3-Gallate and Melatonin on Familial Alzheimer's Disease *PSEN1 E280A* Cerebral Spheroids Derived from Menstrual Mesenchymal Stromal Cells

Viviana Soto-Mercado, Miguel Mendivil-Perez, Carlos Velez-Pardo* and Marlene Jimenez-Del-Rio*
Neuroscience Research Group, Medical Research Institute, Faculty of Medicine, University of Antioquia, SIU Medellin, Colombia

Accepted 18 January 2023
Pre-press 24 February 2023

Abstract.

Background: Familial Alzheimer's disease (FAD) is caused by mutations in one or more of 3 genes known as *AβPP*, *PSEN1*, and *PSEN2*. There are currently no effective therapies for FAD. Hence, novel therapeutics are needed.

Objective: To analyze the effect of treatment with a combination of epigallocatechin-3-gallate (EGCG) and Melatonin (N-acetyl-5-methoxytryptamine, aMT) in a cerebral spheroid (CS) 3D *in vitro* model of *PSEN1 E280A* FAD.

Methods: We developed a CS *in vitro* model based on menstrual stromal cells derived from wild-type (WT) and mutant *PSEN1 E280A* menstrual blood cultured in *Fast-N-Spheres V2* medium.

Results: Beta-tubulin III, choline acetyltransferase, and GFAP in both WT and mutant CSs spontaneously expressed neuronal and astroglia markers when grown in *Fast-N-Spheres V2* medium for 4 or 11 days. Mutant *PSEN1* CSs had significantly increased levels of intracellular *AβPP* fragment peptides and concomitant appearance of oxidized DJ-1 as early as 4 days, and phosphorylated tau, decreased $\Delta\Psi_m$, and increased caspase-3 activity were observed on Day 11. Moreover, mutant CSs were unresponsive to acetylcholine. Treatment with a combination of EGCG and aMT decreased the levels of all typical pathological markers of FAD more efficiently than did EGCG or aMT alone, but aMT failed to restore Ca^{2+} influx in mutant CSs and decreased the beneficial effect of EGCG on Ca^{2+} influx in mutant CSs.

Conclusion: Treatment with a combination of EGCG and aMT can be of high therapeutic value due to the high antioxidant capacity and anti-amyloidogenic effect of both compounds.

Keywords: Alzheimer's disease, cerebral spheroids, E280A, (-) epigallocatechin 3-gallate, melatonin, menstrual mesenchymal stromal cell, mutation, presenilin

*Correspondence to: Marlene Jimenez-Del-Rio and Carlos Velez-Pardo, Neuroscience Research Group, Medical Research Institute, Faculty of Medicine, University of Antioquia (UdeA), Calle 70 No. 52-21, and Calle 62 #52-59, Building 1,

Room 412; SIU Medellin, Colombia. E-mails: marlene.jimenez@udea.edu.co, and calberto.velez@udea.edu.co; ORCID: 0000-0003-3477-2386, 0000-0002-0557-0411.

INTRODUCTION

Familial Alzheimer's disease (FAD) is caused by mutations in one or more of at least three genes known as amyloid- β protein precursor (*A β PP*), presenilin 1 (*PSEN1*), and presenilin 2 (*PSEN2*) (<https://www.alzforum.org/mutations>). A β PP, a transmembrane protein, is cleaved to form amyloidogenic A β peptides (mostly A β_{42}), and presenilin, a subunit of γ -secretase, is the aspartyl protease responsible for A β_{42} generation [1]. To date, 350 different *PSEN1* mutations have been reported to cause FAD (<https://www.alzforum.org/mutations/psen-1>). A missense mutation at position 73664808 on chromosome 14, A>C (codon change: GAA to GCA, exon 8), results in a change in *PSEN1* Glu280Ala (p. E280A) [2]. This mutation has been shown to cause familial early onset Alzheimer's disease (EOAD) in a large family in Colombia [3]. The *PSEN1 E280A* mutation results in the production of extracellular plaques consisting of A β_{42} [4, 5], loss of hippocampal neurons [6], and accumulation and hyperphosphorylation of tau protein (p-tau) [7, 8] and also induces cerebellar A β plaque deposition [9]. Of note, the "paisa" *E280A* mutation provokes accumulation of A β plaque in cognitively unaffected carriers of the *PSEN1 E280A* mutation ten years before autosomal dominant FAD is clinically detectable [10]. Unfortunately, although clinical trials of investigational disease-modifying drugs that target A β have been conducted (ClinicalTrials.gov, NCT01998841) [11], no effective therapies against FAD have become available. Hence, innovative therapeutic approaches are currently needed.

Mesenchymal stromal cells (MSCs) are multipotent cells that have the potential to differentiate into mesodermal, endodermal, or ectodermal cell lineages [12, 13]. Therefore, MSCs are not only important for modeling FAD [14] but are also useful in the assessment of potential therapeutic methodologies (e.g., [15]). Given that MSCs can be obtained from menstrual blood (MensB) without bioethical constraints and/or increasing the likelihood of tumor formation [16], these cells have surfaced as a source for 3D *in vitro* modeling [17, 18] and a potential source for AD treatment [19]. Accordingly, we used menstrual stromal cells (MenSCs) from MensB to obtain cerebral spheroids (CSs), i.e., free-floating spherical conglomerates, within 4 days [20] by growth of the cells in *Fast-N-Spheres* medium [21]. However, there is no further information at present regarding whether MenSCs that carry the *PSEN1 E280A* muta-

tion can generate CSs or regarding whether they are able to reproduce the classical neuropathological features of FAD, i.e., accumulation of intracellular A β PP fragments (iA β PPf), oxidative stress (OS), and tau phosphorylation (p-tau), as has been demonstrated in a 2D *in vitro* model [22].

We recently showed that epigallocatechin-3-gallate (EGCG) represses the accumulation of iA β PPf, blocks tau phosphorylation, enhances mitochondrial membrane potential ($\Delta\Psi_m$), decreases oxidation of the stress sensor protein DJ-1 (oxDJ-1), and inhibits the expression of cell death markers (e.g., c-JUN, TP53, PUMA, and CASP3) in *PSEN1 E280A* cholinergic-like neurons (ChLNs) compared to wild-type (WT) cells in 2D *in vitro*. Although EGCG did not significantly reduce extracellular (e)A β_{42} (although it decreased aggregation of eA β_{42}), it significantly inhibited Ca²⁺ influx impairment in response to acetylcholine (ACh) in *PSEN1 E280A* ChLNs [23]. Melatonin (N-acetyl-5-methoxytryptamine, aMT), a hormone that possesses antioxidant activity [24], has been found to alleviate OS [25], A β accumulation [26, 27], tau pathology [28], and decreased mitochondrial dysfunction [29] by acting as a neuroprotectant [30]. However, it is unknown whether aMT protects *PSEN1 E280A* CSs from endogenously generated iA β PPf, tau phosphorylation, OS, apoptosis, or Ca²⁺ influx dysfunctionality. We hypothesize that single or combined treatment with EGCG and confers neuroprotection against A β -induced pathology in a 3D *in vitro* model of FAD.

Here, we wanted to examine whether *PSEN1 E280A* MenSCs differentiate into CSs when cultured in *Fast-N-Spheres V2* medium, a novel medium that was originally developed and named in our laboratory, and to determine whether treatment with EGCG and/or aMT alone or in combination decreases the levels of pathological markers in *PSEN1 E280A* CSs. Similar to 2D cultured cells, mutant MenSCs can be converted into *PSEN1 E280A* CSs by growth in *Fast-N-Spheres V2* medium for 4 or 11 days. The *PSEN1 E280A* CSs, but not WT *PSEN1* CSs, showed signs of increased accumulation of iA β PPf (detected using antibody E610) and increased phosphorylation of tau at Ser²⁰²/Thr²⁰⁵ (detected using antibody AT8). Mutant CSs, but not WT CSs, molecularly mimic FAD. *PSEN1 E280A* CSs displayed signs of OS as early as 4 days, as demonstrated by the appearance of DJ-1Cys¹⁰⁶-SO₃ and of apoptotic markers such as caspase 3 (CASP3), and concomitant loss of $\Delta\Psi_m$; however, CSs contained p-tau at Day 11. Mutant

CSs also showed Ca^{2+} flux dysregulation compared to control (WT) CSs. Interestingly, exposure of the cells to EGCG and aMT alone or in combination decreased OS and the expression of apoptotic markers, increased $\Delta\Psi_m$, and blocked p-tau in *PSEN1 E280A* CSs. However, EGCG was much more efficient at reversing Ca^{2+} influx dysregulation in *PSEN1 E280A* CSs than was aMT alone or the combination of EGCG/aMT. Our findings demonstrate that EGCG is by far the most efficient neuroprotective agent against endogenously generated pathological iA β PPf, OS, and p-tau in *PSEN1*-derived CSs. Combined treatment with EGCG and aMT can be of high therapeutic value in alleviating endogenously generated oxidative stress elicited by iA β PPf in mutant neurons.

MATERIALS AND METHODS

Isolation and characterization of MenSCs derived from human MensB

The MensB samples were collected from one healthy female and one female carrier of the mutation *PSEN1 E280A* aged 30 years (Tissue Bank Code, TBC # 69308) and 25 years (TBC # 04335), respectively. Donors signed an informed consent accepted by the Ethics Committee of the Sede de Investigación Universitaria -SIU-, University of Antioquia, Medellín, Colombia. The specimens (MensB) were collected, purified, and maintained as previously described in [20]. The isolated MenSCs were used for the generation of cerebral spheroids [20].

Ethical Approval Menstrual specimen donors provided a signed informed consent approved by the ethics committee of the Sede de Investigación Universitaria (SIU), University of Antioquia, Medellín, Colombia (Act 2020-10854).

Generation of cerebral spheroids derived from MensB-MenSCs and induced to cholinergic-like neuronal cell lineage

CSs were obtained by differentiation of WT or *PSEN1 E280A* MenSCs as previously described in [20]. Briefly, WT and mutant MenSCs were cultured in a brand-new medium called *Fast-N-Spheres V2* composed of serum-free culture medium containing reagents as described in [20] plus Matrigel[®] and 1% fetal bovine serum. Cultures were constantly shaken for 4 and 11 days. The MenSCs-derived CSs were

examined for the expression of neuronal and astrocyte markers according to [20].

Immunofluorescence and fluorescence microscopy analysis

The WT or *PSEN1 E280A* CSs cultured with *Fast-N-Spheres V2* medium for 4 and 11 days without or with EGCG (25 μM) and/or melatonin (50 μM) were stained with primary antibodies against the glial fibrillary acidic protein (GFAP, cat. no. sc6170, Santa Cruz), β -tubulin III (β -TUB III cat. no. G712A, Promega), choline acetyltransferase (ChAT, cat. no. AB144P, Millipore) primary antibodies (1:500); primary antibodies against APP751 and/or protein amyloid β 1–42 (1:500; clone 6E10 cat# 803014, Biogen), oxidized DJ-1 (1:500; ox(Cys¹⁰⁶)DJ-1; spanning residue Cys¹⁰⁶ of human PARK7/DJ1; oxidized to produce cysteine sulfonic (SO_3) acid; cat # ab169520, Abcam), and total tau (1:500; t-Tau; cat# T6402, Sigma), and phospho-tau (p-tau, 1:500, Ser²⁰²/Thr²⁰⁵, cat# MN1020 (AT8), Thermo Fisher Scientific) antibodies. Incubation with secondary fluorescent antibodies and nuclei staining were performed according to [20]. Fluorescent Thioflavin-T derivative BTA-1 staining was performed by incubating CSs slides with a BTA-1 (Sigma) solution (500 nM) for 30 min. Nuclei were identified by incubating CSs with propidium iodide (1 μM). Postmortem temporal cortical slices from an Alzheimer's disease patient (case #3396) and a healthy individual (case #3648) were used as a positive and negative control, respectively [31]. Imaging processing data was performed according to an online guidance program (<https://imagej.nih.gov/ij/>).

Live fluorescence analysis

The WT or *PSEN1 E280A* CSs cultured with *Fast-N-Spheres V2* medium for 11 days without or with EGCG (25 μM) and/or melatonin (50 μM) were incubated with (20 nM) MitoTracker[™] Red FM (cat. no. M22425, Invitrogen) and 1X Vybrant TM FLICA (Thermo Fisher Scientific, cat: V35118) according to [20]. Fluorescence microscopy photographs were taken using a Zeiss AxioStart 50 Fluorescence Microscope equipped with a Zeiss AxioCam Cm1 (Zeiss Wöhlk-Contact-Linsfluoreen, Gmb Schöckirchen, Germany), and imaging processing data was performed according to an online guidance program (<http://imagej.nih.gov/ij/>).

Flow cytometry analysis

Flow cytometry analysis was performed according to [32] with minor modifications. Briefly, the WT or *PSEN1 E280A* CSs cultured with *Fast-N-Spheres V2* medium for 11 days without or with EGCG (25 μ M) and/or melatonin (50 μ M) were detached with Accutase Cell Detachment Solution (Beckton Dickinson) and washed in PBS. Cells (10×10^5) were resuspended in PBS and fixated with cold ethanol overnight and used for further flow cytometry analysis. Cell markers were analyzed by incubating cells with primary antibodies against caspase-3 (1:250; cat # AB3623, Millipore), APP751 and/or protein amyloid- β 1-42 (1:500; clone 6E10 cat# 803014, Biogen), oxidized DJ-1 (1:500; ox(Cys¹⁰⁶)DJ-1; spanning residue Cys¹⁰⁶ of human PARK7/DJ1; oxidized to produce cysteine sulfonic (SO₃) acid; cat # ab169520, Abcam), and total tau (1:500; t-Tau; cat# T6402, Sigma), and phospho-tau (p-tau, 1:500, Ser²⁰²/Thr²⁰⁵, cat# MN1020 (AT8), Thermo Fisher Scientific) antibodies, followed incubation with secondary fluorescent antibodies according to [23]. Resuspended cells were analyzed using BD LSR Fortessa II flow cytometer (BD Biosciences). Ten thousand events were acquired, and the acquisition analysis was performed using FlowJo 7.6.2 Data Analysis Software.

Cytochemical detection of DNA fragmentation

DNA fragmentation was determined in fixed untreated or treated CSs to polylysine coated slides by the terminal deoxynucleotidyl transferase dUTP nick end labeling (TUNEL) technique according to the manufacturer's protocol (Promega catalog #G7130). Briefly, CSs samples were treated for 10 min with 25 μ g/ml protease K and fixed in 4% methanol in PBS for 5 min. CSs slides were pre-incubated with equilibration buffer (EB) (50 μ l, 200 mM potassium cacodylate, pH 6.5; 25 mM Tris-HCl pH 6.6; 0.2 mM DTT; 0.25 mg/ml BSA; 2.5 mM cobalt chloride) for 15 min. Then, slides were incubated at 37°C for 60 min with 25 μ l TdT incubation buffer (23 μ l EB; 2 μ l nucleotide mix; 0.5 μ l TdT enzyme). After the appropriate incubation time, tailing reaction was terminated by immersing the slides in 2X SSC for 15 min and rinsing twice with PBS. Then after, slides were incubated with streptavidin HRP (diluted 1:500 in PBS) for 30 min at room temperature. Finally, slides were incubated with DAB solution (prepared immediately prior to use by adding 100 μ l DAB 10X

Chromogen to 900 μ l DAB Substrate 1X Buffer). Slides were stained with safranin for 10 s at room temperature and washed twice in deionized water. Immediately, slides were coverslipped using aqueous mounting media.

Oxygen radical absorbance capacity (ORAC) assay

The hydrophilic ORAC assay was performed as described in [33]. The AAPH (2,2'-Azobis(2-amidinopropane) dihydrochloride) was used as a peroxy radical generator, Trolox was used as a standard, and fluorescein was used as the fluorescent probe. Briefly, fluorescein, AAPH, and the samples were prepared in a phosphate buffer (75 mM, pH 7.4). First, 25 μ L of sample solution or Trolox standard was mixed with 150 μ L of fluorescein (1 mM) and pre-incubated at 37°C for 30 min before the addition of 25 μ L of AAPH solution (200 mM). The fluorescence at an excitation wavelength of 485 nm and an emission wavelength of 520 nm was measured every 2 min for 120 min using a Synergy HT Multi-Mode Microplate Reader (BioTek Instruments, Inc.; Winooski, USA). The relative ORAC values were calculated using the differences of areas under the decay curves and were expressed as μ mol Trolox equivalents (TE)/g of solution.

Intracellular calcium imaging

The cytoplasmic Ca²⁺ concentration ([Ca²⁺]_i) was measured according to Pap et al. [34]. Fluorescence microscopy photographs were taken using a Zeiss AxioStart 50 Fluorescence Microscope equipped with a Zeiss AxioCam Cm1 (Zeiss Wöhlk-Contact-Linsfluoreen, Gmb Schöckirchen, Germany), and imaging processing data was performed according to online guidance program (<http://imagej.nih.gov/ij/>) [35].

Data analysis

This experimental design was performed as previously reported in [20] and based on the statistics considerations described in [36]. Provided that the experimental unit (i.e., the well) data fulfill the independence of observations, the dependent variable is normally distributed in each treatment group (Shapiro-Wilk test), and variances are homogeneous (Levene's test), the statistical significance was deter-

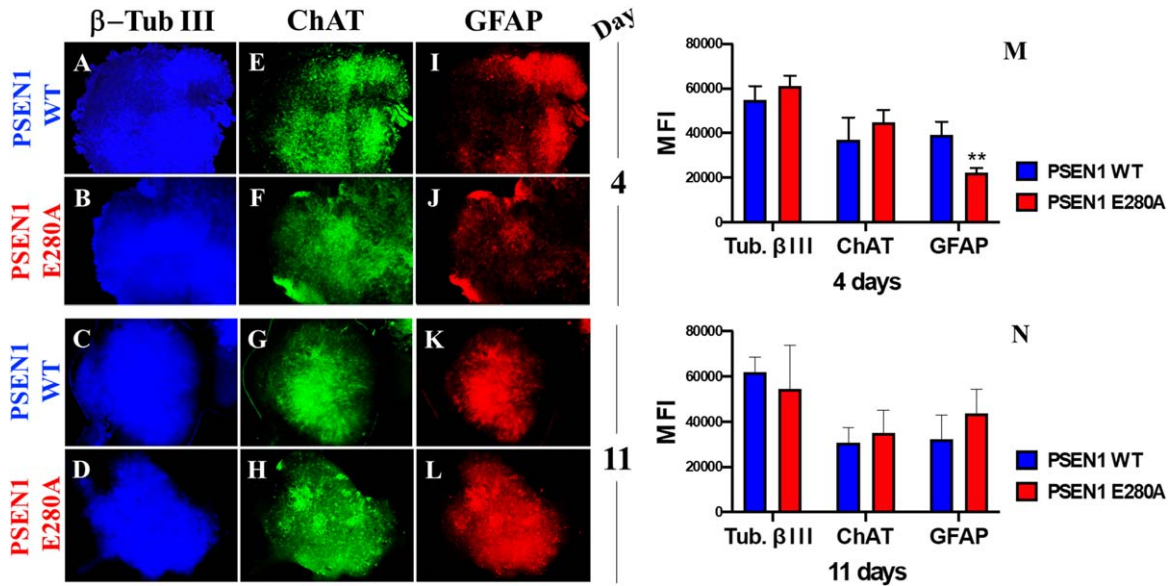


Fig. 1. MenSCs-derived CSs show cholinergic and astrocytic marker. After 4 and 11 days, WT *PSEN1* and *PSEN1 E280A* CSs were triple-stained as indicated in the figure with primary antibodies against β -TUB III (blue; A–D), ChAT (green; E–H), and GFAP (red; I–L). M) Mean fluorescence intensity (MFI) quantification of images obtained by immunofluorescence analysis on day 4. N) MFI quantification of images obtained by immunofluorescence analysis on day 11. Images represent one out of three independent experiments. Statistical significance was determined by one-way ANOVA with a Tukey *post hoc* test; ** $p < 0.01$. Image magnification 10x.

mined by *Student's t*-test, one-way, or two-way ANOVA followed by Bonferroni's or Tukey's *post hoc* comparison calculated with GraphPad Prism 5.0 software. Differences between groups were only deemed significant when a p -value of <0.05 (*), <0.001 (**), and <0.001 (***). All data are illustrated as the mean \pm S.D.

RESULTS

PSEN1 E280A CSs spontaneously express cholinergic and astrocytic markers

Previous work has shown that WT CSs derived from MensB spontaneously express neuronal markers such as β -TUB III and ChAT, as well as the astrocyte marker GFAP, when cultured in *Fast-N-Spheres* medium for 3 days [20]. Likewise, WT and *PSEN1 E280A* CSs showed similar expression of neuronal (β -TUB III, Fig. 1A–D), cholinergic (ChAT, Fig. 1E–H), and astrocytic (GFAP, Fig. 1I–L) lineage cell markers when grown in *Fast-N-Spheres V2* medium for 4 (Fig. 1M) or 11 days (Fig. 1N).

PSEN1 E280A CSs show an early increase in iA β PPf and OS

Next, we wanted to determine whether CSs express the typical neuropathological features of AD, such as A β and OS. Figure 2 shows that WT NS displayed neither iA β PPf accumulation (Fig. 2A, C) nor OS markers (Fig. 2E, G), as reflected by the absence of iA β PPf (Fig. 2M, N), oxidized protein DJ-1 (Fig. 2M, N) and nuclear-positive cells (Fig. 2I–L). In contrast, *PSEN1 E280A* CSs displayed enhanced iA β PPf (Fig. 2B, D, M, N) and oxidation of protein DJ-1 (Fig. 2F, H, M, N) as early as 4 days in culture (Fig. 2M, N).

PSEN1 E280A CSs present hyperphosphorylation of tau protein

It is well established that phosphorylation of tau occurs downstream of A β pathology in AD [37, 38]. Therefore, we assessed whether tau is phosphorylated in a time-dependent manner in mutant CSs. As shown in Fig. 3, no p-tau was observed in WT CSs (Fig. 3A, C) on Days 4 or 11, whereas p-tau was detected in *PSEN1 E280A* CSs only on Day 11 (Fig. 3B versus

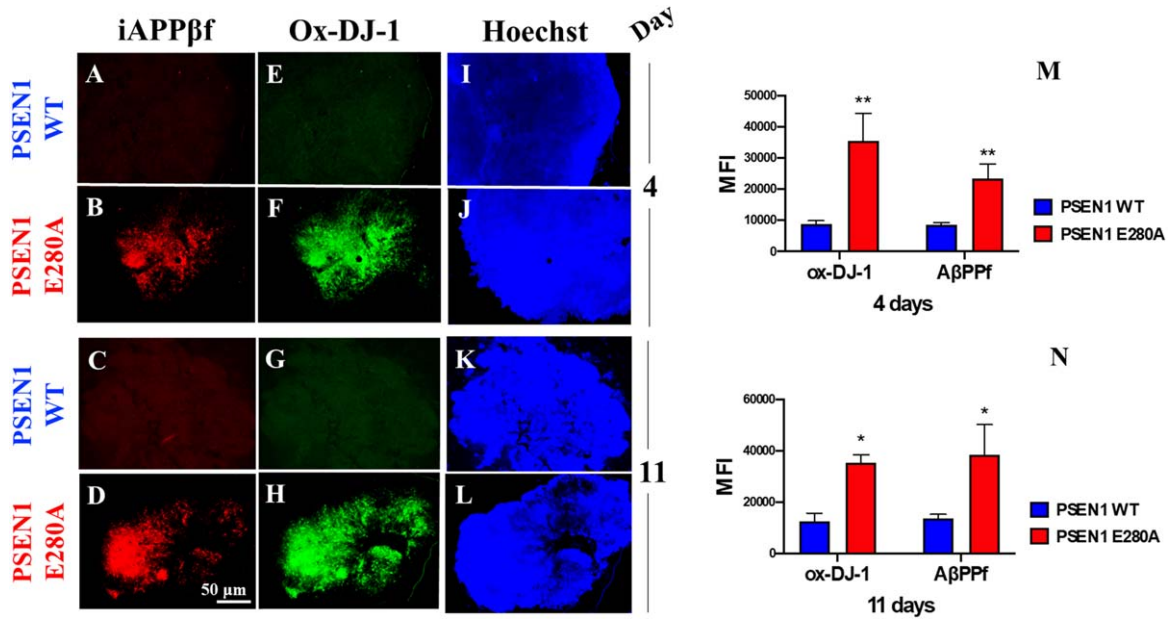


Fig. 2. *PSEN1 E280A* cerebral spheroids (CSs) accumulate intracellular AβPP fragments (iAβPPf) and oxidized (Cys¹⁰⁶) DJ-1 protein (Ox-DJ-1). After 4 and 11 days, WT *PSEN1* and *PSEN1 E280A* CSs were double-stained in the figure with primary antibodies against (i)AβPPf (red; A–D) and Ox-DJ-1 (green; E–H). Nuclei were stained with Hoechst (blue; I–L). M) Mean fluorescence intensity (MFI) quantification of images obtained by immunofluorescence analysis on day 4. N) MFI quantification of images obtained by immunofluorescence analysis on day 11. Images represent one out of three independent experiments. Statistical significance was determined by one-way ANOVA with a Tukey *post hoc* test; **p* < 0.05; ***p* < 0.01. Image magnification 10x.

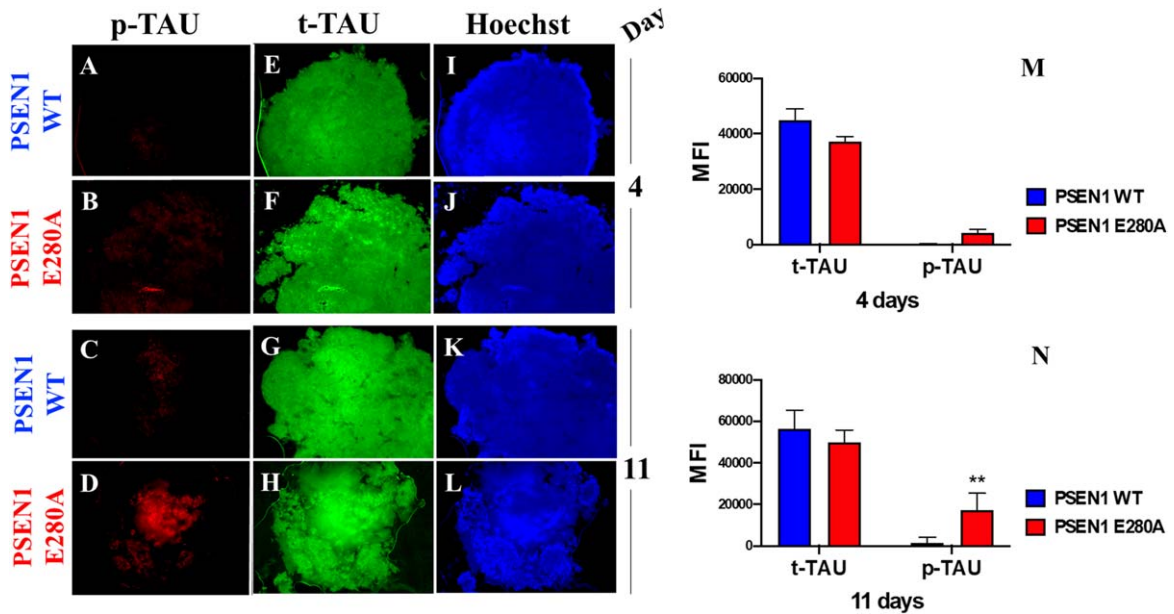


Fig. 3. *PSEN1 E280A* cerebral spheroids (CSs) show hyperphosphorylation of protein tau. After 4 and 11 days, WT *PSEN1* and *PSEN1 E280A* CSs were double-stained as indicated in the figure with primary antibodies against phosphorylated (Ser²⁰²/Thr²⁰⁵) Tau (p-Tau) (red; A–D) and total Tau (t-Tau) (green; E–H). Nuclei were stained with Hoechst (blue; I–L). M) Mean fluorescence intensity (MFI) quantification of images obtained by immunofluorescence analysis on day 4. N) MFI quantification of images obtained by immunofluorescence analysis on day 11. Images represent one out of three independent experiments. Statistical significance was determined by one-way ANOVA with a Tukey *post hoc* test; ***p* < 0.01. Image magnification 10x.

Fig. 3D and 3M versus 3N). Total tau was measured and used for protein normalization (Fig. 3E–H), and Hoechst staining was used to analyze the organoid cellularity (Fig. 3I–L).

PSEN1 E280A CSs show diminished $\Delta\Psi_m$, caspase 3 activity, and fragmented nuclei

We then wondered whether *PSEN1 E280A* CSs show endogenous alterations in $\Delta\Psi_m$, active CASP-3 and nuclear fragmentation similar to those demonstrated in 2D *PSEN1 E280A* human umbilical cord Wharton Jelly mesenchymal stromal cell-derived ChLNs [22]. Figure 4 shows that WT CSs displayed high $\Delta\Psi_m$, inactive CASP3 and intact nuclei (Fig. 4A, E). However, *PSEN1 E280A* CSs displayed typical features of apoptotic cells, including failure of $\Delta\Psi_m$, CASP3-positive signals, and broken nuclei (Fig. 4F, J). Similar observations were obtained by flow cytometry (Fig. 4K, L) and the TUNEL technique (Fig. 4M, Q, R, W).

*Combined treatment with EGCG and aMT increases $\Delta\Psi_m$ and drastically reduces caspase 3 activation in *PSEN1 E280A* CSs*

Previous work has shown that EGCG diminishes amyloid-induced cytotoxic effects on 2D *PSEN1 E280A* ChLNs derived from hUC-WJ MSCs [22] and that the hormone aMT acts as a neuroprotectant [30, 39]. Therefore, we determined the effect of polyphenols and hormones on mitochondrial functionality in CSs. As shown in Fig. 4, EGCG only (Fig. 4B), aMT only (Fig. 4C), or a combination of the two (Fig. 4D) induced neither alteration in the $\Delta\Psi_m$ nor activation of the executor protein CASP3 in WT CSs (Fig. 4E) compared to untreated CSs (Fig. 4A, E). Remarkably, treatment with EGCG only (Fig. 4G), aMT only (Fig. 4H), or a combination of the two (Fig. 4I) significantly increased $\Delta\Psi_m$ compared to untreated *PSEN1 E280A* CSs (Fig. 4F), and these treatments were equally efficient in reducing CASP3 activation in mutant CSs (Fig. 4E versus 4J). Similar results were obtained by flow cytometry (Fig. 4K, L) and the TUNEL technique (Fig. 4N–Q, S–W).

*Combined treatment with EGCG and aMT dramatically diminishes iA β PPf and OS levels in *PSEN1 E280A* CSs*

Based on the above observations, we were prompted to assess whether EGCG and aMT alone

or in combination can reverse the neuropathologic features of FAD in mutant CSs. To determine this, WT CSs and *PSEN1 E280A* CSs were left untreated (used as control) or incubated with EGCG at 25 μ M, a pharmacological concentration of aMT (50 μ M) or a combination of EGCG and aMT. As illustrated in Fig. 5, EGCG, aMT, and EGCG/aMT were innocuous to WT CSs (Fig. 5A versus Fig. 5B–E). However, aMT (Fig. 5H, J) was significantly more effective than EGCG alone in preventing the accumulation of iA β PPf in *PSEN1 E280A* CSs (Fig. 5G, J), and treatment with a combination of the two reduced the level of iA β PPf in mutant CSs (Fig. 5I, J) to nearly control values, i.e., those found in WT CSs. In contrast, EGCG was much more effective than aMT in reducing the oxidation of the sensor protein DJ-1 (Fig. 5F versus Fig. 5G and 5J). The combination of the two drugs was even more effective than EGCG alone in reducing OS in mutant CSs (Fig. 5F versus Fig. 5I and J). Flow cytometry analysis yielded comparable results (Fig. 5K–T).

To further confirm that the thwarting effect of the molecules was specifically on iA β PP and not on extracellular A β aggregates, we stained WT and mutant CSs with thioflavin BTA-1, a specific fluorescent thioflavin-T derivative that has high affinity for amyloid deposits and specifically labels β -amyloid aggregates. BTA-1 displays 50-fold higher affinity for A β aggregates than does thioflavin-T, selectively stains A β fibrils in postmortem brain tissue obtained from AD patients and crosses the blood-brain barrier. We also stained postmortem temporal cortical samples obtained from individuals with normal and *E280A* mutant *PSEN1* as internal negative and positive controls, respectively. As expected, the mutant *E280A* temporal postmortem sample displayed typical amyloid plaques (Fig. 5V, arrowheads) and A β fibrils (Fig. 5V, asterisks), but such plaques were completely absent from the WT temporal postmortem sample (Fig. 5U). Interestingly, untreated or treated WT or mutant CSs showed neither BTA-1-positive staining for amyloid plaques nor A β fibrils (Fig. 5W–AD).

Simultaneously, we wanted to determine whether the reduction in DJ-1 oxidation via H₂O₂ activation might be due to antioxidant activity of EGCG and aMT when incubated with CSs. The ORAC assay (also known as the hydrogen atom transfer (HAT)-based assay) showed that EGCG, aMT and combined EGCG/aMT displayed high antioxidant activity, yielding values of 37,870.75 \pm 671.43 μ mol Trolox equivalents (TE)/g, 55,822.86 \pm 585.18 μ mol

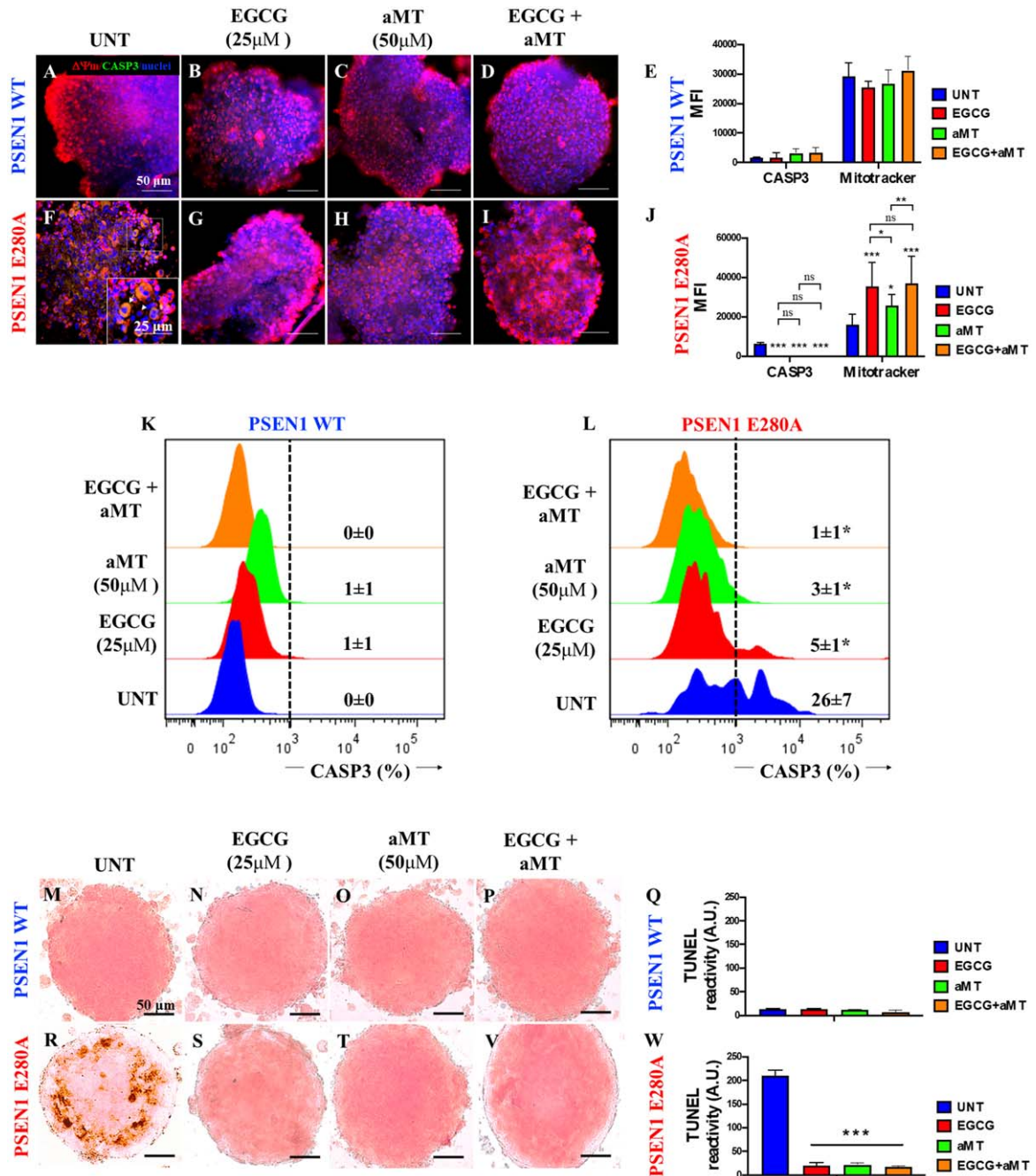


Fig. 4. Combined treatment with EGCG and aMT reestablish mitochondria membrane potential ($\Delta\Psi_m$), inactivate CASPASE-3 activation, and block nuclei fragmentation in *PSEN1 E280A* (CSs). The WT *PSEN1* and *PSEN1 E280A* CSs were left without (UNT; A, F) or treated with 25 μ M EGCG (B, G) and 50 μ M aMT (C, H) alone or in combination (D, I) until day 11. CSs were triple stained as indicated in the figure with MitoTracker™ Red FM (red), 1X Vybrant™ TM FLICA (green), and Hoechst (blue). E) Mean fluorescence intensity (MFI) quantification of images obtained by immunofluorescence analysis of *PSEN1* WT CSs. J) MFI quantification of images obtained by immunofluorescence analysis of *PSEN1 E280A* CSs. K, L) representative histograms of WT *PSEN1* (K) and *PSEN1 E280A* CSs (L) treated with none (UNT) or with EGCG, aMT, and EGCG/aMT. M-P, R-V) The WT *PSEN1* and *PSEN1 E280A* CSs were left without (UNT; M, R) or treated with EGCG (N, S), aMT (O, T), or in combination (P, V) for 11 days. Then, untreated or treated CS were TUNEL stained. Only untreated *PSEN1 E280A* CSs (R) show TUNEL-positive cells. Q, W) TUNEL reactivity quantification of images obtained by TUNEL technique analysis after 11 days. Histograms and images represent one out of three independent experiments. Statistical significance was determined by one-way ANOVA with a Tukey *post hoc* test; * $p < 0.05$; *** $p < 0.001$. Image magnification 10x.

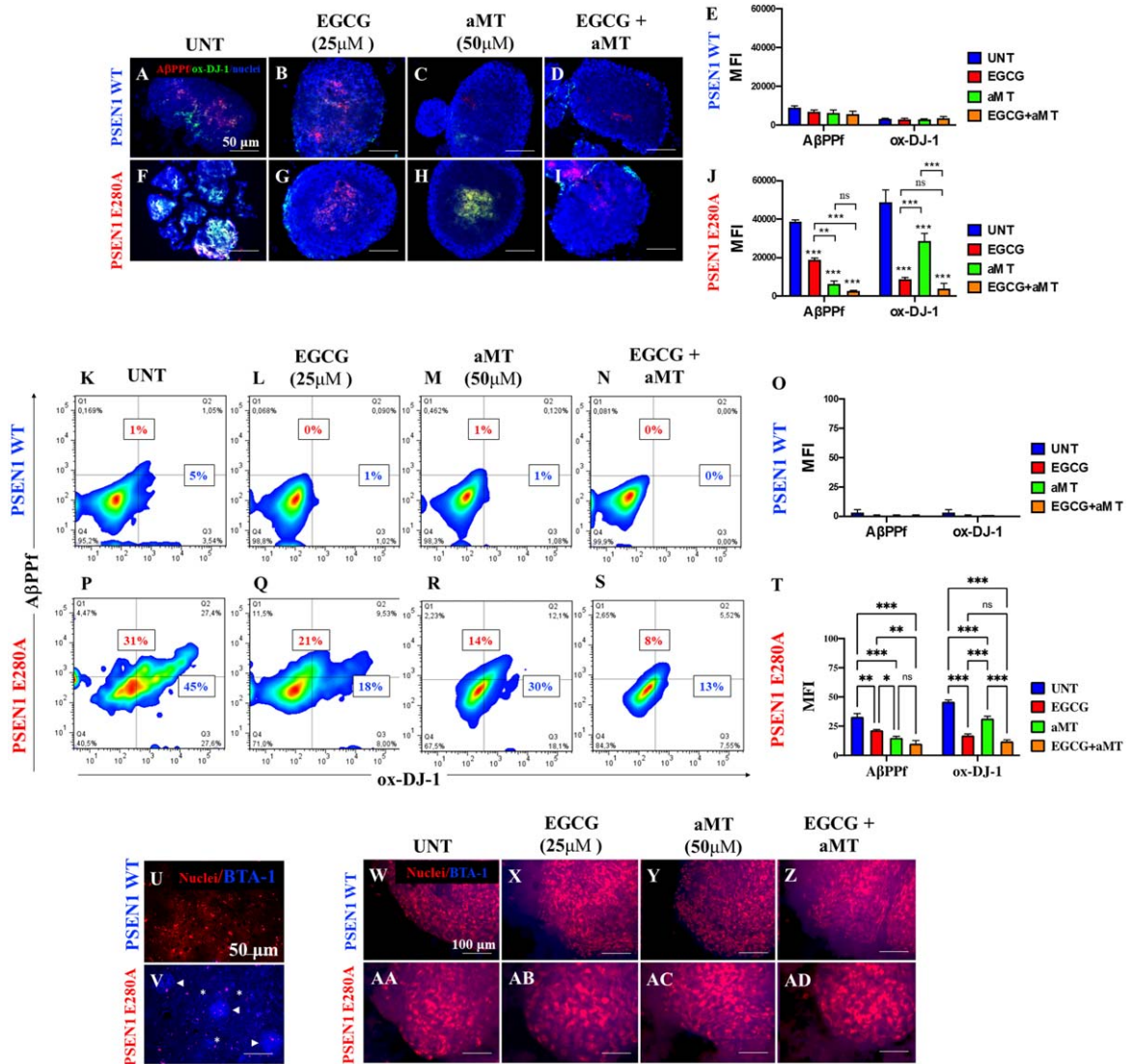


Fig. 5. Combined treatment with EGCG and aMT reduce iAβPPf and OS in *PSEN1 E280A* CSs. The WT *PSEN1* and *PSEN1 E280A* CSs were left without (UNT; A, F) or treated with 25 μM EGCG (B, G) and 50 μM aMT (C, H) alone or in combination (D, I) for 11 days. CSs were double-stained as indicated in the figure with antibodies against sAβPPf (red) and Ox-DJ-1 (green), and nuclei were stained with Hoechst (blue). E) Mean fluorescence intensity (MFI) quantification of images obtained by immunofluorescence analysis of *PSEN1* WT CSs. J) MFI quantification of images obtained by immunofluorescence analysis of *PSEN1 E280A* CSs. K-N, P-S) Representative 2D density plot showing iAβPPf (y-axis) and ox-DJ-1 (x-axis) flow cytometry double analysis performed on untreated WT (K) and mutant CSs (P), or treated with EGCG only (L, Q), aMT only (M, R), and EGCG/ aMT (N, S). O, T) represent the quantitative analysis of the data from quadrant Q1 + Q2 for iAβPPf and Q2 + Q4 for ox-DJ-1. U-V) represent BTA-1 negative staining of a temporal cortex sample from a healthy individual (case #3648) and BTA-1 positive staining of a temporal cortex sample from a *PSEN1 E280A* individual (case #3396). Arrowheads show Aβ plaques, and asterisks show Aβ fibrils. W-AD) The WT *PSEN1* and *PSEN1 E280A* CSs were left without (UNT; W, AA) or treated with EGCG (X, AB) and aMT (Y, AC) alone or in combination (Z, AD) for 11 days. Then, CSs were double stained with BTA-1 and propidium iodide as indicated in the figure. BTA-1 negative staining was observed in untreated or treated CSs. Except for Fig. 5U and 5V, 2D histograms and images represent one out of three independent experiments. Statistical significance was determined by one-way ANOVA with a Tukey *post hoc* test; ****p* < 0.001. Image magnification 10x.

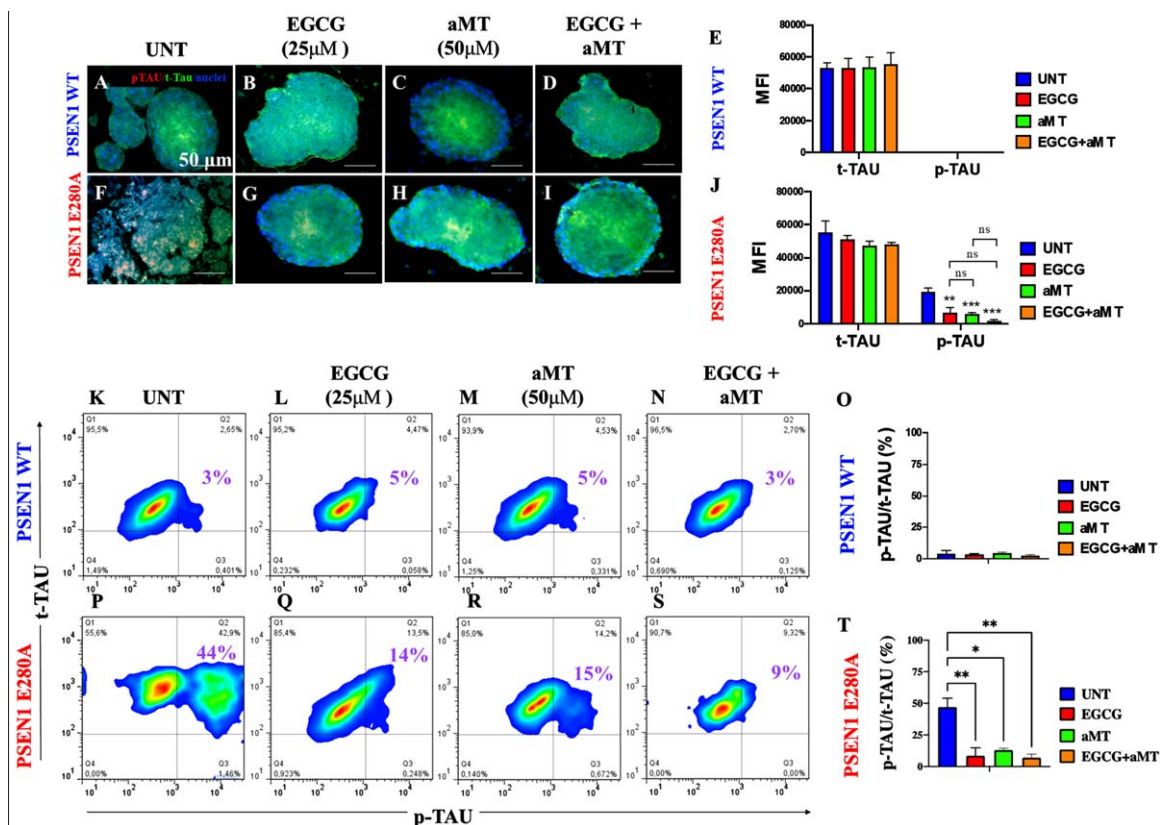


Fig. 6. Combined treatment with EGCG and aMT completely blocked the phosphorylation of protein tau. WT *PSEN1* and *PSEN1 E280A* CSs were left without (UNT; A, B) or treated with 25 μ M EGCG (C, D) and 50 μ M aMT (E, F) alone or in combination (G, H) for 11 days. CSs were double-stained as indicated in the figure with antibodies against phosphorylated (Ser²⁰²/Thr²⁰⁵) Tau (p-Tau; red), total Tau (t-Tau; green), and nuclei were stained with Hoechst (blue). I) Mean fluorescence intensity (MFI) quantification of images obtained by immunofluorescence analysis of *PSEN1* WT CSs. J) MFI quantification of images obtained by immunofluorescence analysis of *PSEN1 E280A* CSs. K-N, P-S) Representative 2D density plot showing t-tau (y-axis) and p-tau (x-axis) flow cytometry double analysis performed on untreated WT (K) and mutant CSs (P), or treated with EGCG only (L, Q), aMT only (M, R), or EGCG/ aMT (N, S). O, T) represent the quantitative analysis of the data from quadrant Q2. The 2D histograms and images represent one out of three independent experiments. Statistical significance was determined by one-way ANOVA with a Tukey *post hoc* test; ** $p < 0.01$; *** $p < 0.001$. Image magnification 10x.

TE/g, and $130,894.34 \pm 2,874.21 \mu\text{mol TE/g}$, respectively. The mixture showed 3.35-fold and 2.34-fold increases in ORAC values, respectively.

Combined treatment with EGCG and aMT completely blocks phosphorylation of tau protein

We further evaluated whether exposure of CSs to polyphenols, hormones, or a combination of the two is able to decrease p-tau. As shown in Fig. 6, compared to untreated CSs (Fig. 6A, E), no p-tau was observed in WT CSs treated with EGCG (Fig. 6B, E), aMT (Fig. 6C, E), or EGCG/aMT (Fig. 6D, E). When mutant CSs (Fig. 6F) were exposed to these agents, both EGCG alone (Fig. 6G, J) and aMT alone (Fig. 6H, J) significantly diminished p-tau compared to the level found in untreated mutant CSs (Fig. 6J).

Interestingly, treatment with combined EGCG/aMT completely eliminated p-tau (Fig. 6I, J). Flow cytometry yielded similar results (Fig. 6K–T).

When applied together with EGCG, aMT limits the beneficial effect of EGCG on Ca^{2+} influx in *PSEN1 E280A* CSs

Finally, we evaluated the effects of the two compounds on Ca^{2+} functionality in CSs exposed to acetylcholine (ACh). To this end, WT and mutant *PSEN1 E280A* CSs were exposed to ACh at 1 mM final concentration. As shown in Fig. 7, ACh stimulated a temporary increase in intracellular Ca^{2+} in WT CSs (Fig. 7A, $\Delta F/F = 0.165 \pm 0.06$, mean duration = 10 s; $n = 9$ CSs imaged, $N = 3$ dishes Fig. 7E). Ca^{2+} influx into WT CSs after ACh addition was

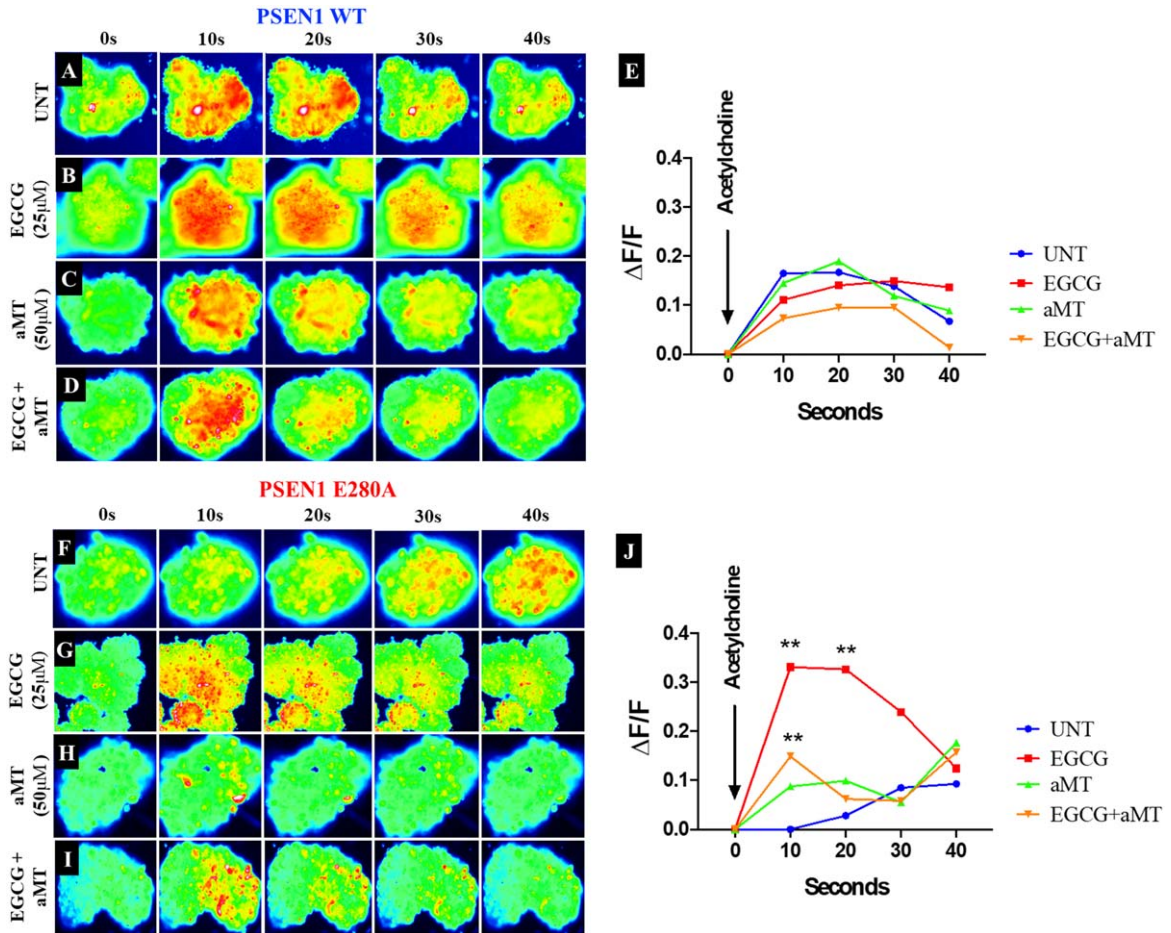


Fig. 7. aMT lessens the effect of EGCG on Ca^{2+} influx in *PSEN1 E280a* CSs. The WT *PSEN1* and *PSEN1 E280A* CSs were left without (UNT; A, F) or treated with 25 μM EGCG (B, G) and 50 μM aMT (C, H) alone or in combination (D, I) until day 11. Time-lapse images (0, 10, 20, 30, and 40 s) of Ca^{2+} fluorescence in CSs ($n=9$ CSs imaged, $N=3$ dishes) as a response to ACh treatment. ACh was puffed into the culture at 0 s (arrow). Then, the Ca^{2+} fluorescence of cells was monitored at indicated times. Color contrast indicates fluorescence intensity: dark blue < light blue < green < yellow < red. E) Normalized mean fluorescence signal ($\Delta F/F$) over time, indicating temporal cytoplasmic Ca^{2+} elevation in response to ACh treatment in *PSEN1* WT CSs. J) Normalized mean fluorescence signal ($\Delta F/F$) over time, indicating temporal cytoplasmic Ca^{2+} elevation in response to ACh treatment in *PSEN1 E280A* CSs. Statistical significance was determined by two-way ANOVA with a Tukey *post hoc* test; ** $p < 0.01$. Image magnification 10x.

altered by EGCG (Fig. 7B), aMT (Fig. 7C), and by a combination of EGCG and aMT (Fig. 7D, E). In contrast, ACh did not affect intracellular Ca^{2+} in mutant *PSEN1* CSs (Fig. 7F, $\Delta F/F = 0.00 \pm 0.02$, mean duration = 10 s; $n=9$ CSs imaged, $N=3$ dishes, Fig. 7J). While EGCG dramatically restored Ca^{2+} influx in mutant CSs (Fig. 7G, $\Delta F/F = 0.33 \pm 0.01$, mean duration = 10; $n=9$ CSs imaged, $N=3$ dishes, Fig. 7J), aMT did not restore Ca^{2+} influx in the mutant CSs (Fig. 7H, J), in contrast to its effect on untreated mutant CSs (Fig. 7F, J). Interestingly, administration of EGCG and aMT together decreased ACh-induced Ca^{2+} influx in *PSEN1 E280A* CSs

(Fig. 7I; $\Delta F/F = 0.15 \pm 0.02$, mean duration = 10 s; $n=9$ CSs imaged, $N=3$ dishes, Fig. 7J).

DISCUSSION

Cerebral spheroids are potential *in vitro* models for understanding neuronal dysfunction [40]. We report for the first time that cholinergic-like *PSEN1 E280A* CSs derived from MenB cells replicate the neuropathological hallmarks of FAD in 3D, mirroring previously reported findings in hUC-MSC-derived ChLNs *PSEN1 E280A* cultured in planar (2D) culture [22]. Indeed, mutant CSs, but not WT CSs,

contained high amounts of intracellular A β PPf, OS, and hyperphosphorylated tau protein, as evidenced through immunochemistry using antibodies to E610, DJ-1-sulfonic (SO₃), and AT8, flow cytometry and BTA-1 staining. Because the WT and mutant cells grow in conglomerates, i.e., in cell spheres, the pathological markers were more prominently detectable in 3D than in 2D cultures. This is indeed an advantage of 3D cultures prepared in *Fast-N-Spheres V2* medium. Since we found no differences in the levels of iA β PP fragments, OS markers, or p-tau after 11 days of culture, the replication of neuropathological features of FAD is easier and more cost-effective when MenSC-derived CSs are used rather than cell models based on other cell culture methods (e.g., [41]). Interestingly, a recently described A β -GFP transgenic mouse model of AD, A β -GFP Tg, displays increased A β accumulation inside neurons and tau phosphorylation, among other physiological alterations [42]. Together, these observations suggest that intracellular A β PP fragments or A β ₁₋₄₂, rather than extracellular A β ₄₂ peptide deposition, might represent early-stage pathology in individuals with *PSEN1 E280A* FAD [43]. Furthermore, our observations support the view that the iA β PP fragments identified by antibody 6E10, mass spectrometry [22] and flow cytometry (this work) trigger OS and hyperphosphorylation of intracellular tau protein in a time-dependent manner in CS-derived ChLNs, probably through a mechanism involving JNK kinase [22]. Moreover, the observation that mutant CSs, but not WT CSs, were unresponsive to ACh suggests that the mutant CSs have altered endogenous physiological Ca²⁺ influx. In agreement with previous studies [44], our observations suggest that the accumulation of iA β PP fragments precedes tau pathology. These findings support the idea that iA β PP fragments and/or A β ₄₂ trigger early neurotoxicity in FAD [45, 46] and represent an early stage in the pathology of AD [43]. However, whether iA β PP fragments and/or A β ₄₂ provoke neuronal apoptosis (represented in this work by loss of $\Delta\Psi_m$ and CASP3-positive cells) or necrosis [43] deserves further investigation. Regardless of the mechanism, intracellular A β is increasingly recognized as a prominent player in cholinergic neuronal demise and as a basis for new treatment approaches, e.g., bioactive polyphenols, cannabinoids, and bifunctional anti-(i)amyloid and anti-OS agents [23, 45, 47–49].

We also report here for the first time that EGCG and aMT in combination are highly effective in improving pathological (i.e., iA β PPf and p-tau), OS (i.e., DJ-

1 Cys¹⁰⁶-SO₃), and apoptosis indicators in *PSEN1 E280A* CSs. These observations might be explained by the effect of each of the components of the mixture. Indeed, we found that both EGCG and aMT display high antioxidant capacity and that the antioxidant capacity of the combined EGCG/aMT was even higher (e.g., 3.35-fold and 2.34-fold increases in ORAC value compared to EGCG and aMT, respectively). We found that EGCG blunted the generation of H₂O₂, as reflected by a reduction in the level of oxDJ-1 [50], inhibition of amyloid accumulation [23, 26, 51], increased disassembly of full-length tau protein [52], blockade of the activation of the main apoptosis factors CASP3 and nuclear fragmentation, and increased $\Delta\Psi_m$, and thereby increased the survival of mutant CSs to a similar extent as WT CSs. Likewise, we found that aMT was also highly effective as a neuroprotective agent against intrinsic insults in *PSEN1 E280A* CSs. aMT not only efficiently scavenged H₂O₂ by acting as an antioxidant [53] but also reduced the accretion of iA β PPf, possibly through direct interaction with amyloid, thereby protecting CSs against iA β PPf toxicity [54, 55]. Furthermore, aMT almost completely blocked hyperphosphorylation of tau protein ([56] and references therein), restored $\Delta\Psi_m$ [57], and inhibited iA β PPf-induced apoptosis in mutant CSs by inactivating CASP3 [55, 58]. These observations are consistent with the idea that both the combination of EGCG/aMT and EGCG and aMT individually act as antioxidants, antiamyloidogenic agents, inhibitors of tau aggregation, and blockers of apoptosis. In agreement with previous observations [23], EGCG altered Ca²⁺ influx in response to ACh in *PSEN1 E280A* CSs. However, mutant CSs were almost unresponsive to ACh when exposed to a combination of aMT and EGCG. Moreover, aMT reduced the beneficial effect of EGCG on Ca²⁺ influx in mutant CSs. How aMT affects Ca²⁺ influx in CSs is not yet known. A possible explanation for our observations is that aMT either interacts directly with cholinergic receptors (e.g., nAChR [59]), blocking their interaction with ACh and thereby inhibiting voltage-activated calcium currents [60], or increases Ca²⁺ efflux from CSs. Additional research is required to clarify this issue. Regardless of the mechanism, our results show that aMT does not contribute to the restoration of Ca²⁺ influx in mutant CSs.

Several studies have shown that EGCG is not only an effective antioxidant (e.g., [61]) but that it also possesses anti-amyloidogenic properties [62].

Our current observations support this interpretation. In agreement with others [63–66], we found that EGCG displays high antioxidant activity according to the ORAC test. Furthermore, EGCG significantly reduced iA β PP accumulation. These results suggest that early inhibition of iA β PP and quenching of ROS, specifically H₂O₂, block further signaling that would otherwise lead to cell death. Interestingly, EGCG can be enzymatically modified to enhance its lipophilicity and antioxidant properties [67]. Unfortunately, no information on the antioxidant effects of such compounds on human cells is currently available. Such derivative compounds might be used to help prevent OS-induced neuronal cell death in FAD. Likewise, in agreement with others, we found that aMT displays antioxidant capacity according to the ORAC assay [68, 69]. This might explain why aMT is effective in alleviating OS induced by H₂O₂ in PTr2 cells [70] and in mutant E280A CSs (this work). We showed here, however, for the first time that the combined action of two antioxidant agents, EGCG and aMT, is even more efficient in protecting mutant CSs. However, further experiments are necessary to establish whether the combined action of EGCG and aMT is additive or synergistic [71].

Conclusion

Familial AD, most cases of which are caused by mutations in *PSEN1*, e.g., *PSEN1 E280A*, is a complex neurodegenerative malady in which progressive neuronal deterioration occurs, leading to loss of memory. It is now accepted that intracellular A β , rather than extracellular A β aggregation, is the likely cause of neuronal cell death. We have shown that early generation and accumulation of iA β PP are responsible for initiating cellular events that lead to ROS (H₂O₂) production, hyperphosphorylation of tau, activation of proapoptotic proteins (e.g., CASP 3), alterations in Ca²⁺ influx, and apoptosis in ChLNs [22] and in CSs (this work). It is, therefore, reasonable to assume that drugs designed to eliminate A β -induced signaling cell death targets/or pathological signals may have cooperative (additive or synergistic) effects. Consistent with this view, combined use of EGCG and aMT has proven to be highly useful in almost completely reducing intracellular A β PP, OS, p-tau, loss of $\Delta\Psi_m$, and apoptotic markers in *PSEN1 E280A* CSs. However, aMT and EGCG in combination were ineffective at restoring Ca²⁺ influx in mutant CSs because of their antagonistic action. Therefore, our present observations provide a cautionary note regarding the

use of aMT to restore physiological functions associated with Ca²⁺ influx. However, this limitation might be overcome by delivering EGCG (e.g., [72]) and aMT (e.g., [73]) nanoparticles to specific brain neurons (e.g., cholinergic or pyramidal) that can be directly loaded with the cargo (EGCG and aMT) intracellularly. Further investigation is needed to validate the effectiveness of using combined EGCG and aMT in the early treatment of FAD patients carrying the *PSEN1 E280A* mutation.

ACKNOWLEDGMENTS

We are grateful to the Bioactive Substances Service and Research Group (SIU-UdeA) for ORAC testing.

FUNDING

This work was funded by MinCiencias (grant. no. 1115-807-62912, contract no. 749-2018).

CONFLICT OF INTEREST

The authors have no conflict of interest to report.

DATA AVAILABILITY

All datasets generated for this study are included in the manuscript.

REFERENCES

- [1] Wolfe MS, Miao Y (2022) Structure and mechanism of the γ -secretase intramembrane protease complex. *Curr Opin Struct Biol* **74**, 102373.
- [2] Lalli MA, Cox HC, Arcila ML, Cadavid L, Moreno S, Garcia, G, Madrigal L, Reiman EM, Arcos-Burgos M, Bedoya G, Brunkow ME, Glusman G, Roach JC, Hood L, Kosik KS, Lopera F (2014) Origin of the PSEN1 E280A mutation causing early-onset Alzheimer's disease. *Alzheimers Dement* **10**, S277-S283.e210.
- [3] Lopera F, Ardilla A, Martínez A, Madrigal L, Arango-Viana JC, Lemere CA, Arango-Lasprilla JC, Hincapié L, Arcos-Burgos M, Ossa JE, Behrens IM, Norton J, Lendon C, Goate AM, Ruiz-Linares A, Rosselli M, Kosik KS (1997) Clinical features of early-onset Alzheimer disease in a large kindred with an E280A presenilin-1 mutation. *JAMA* **277**, 793-799.
- [4] Lemere CA, Lopera F, Kosik KS, Lendon CL, Ossa J, Saido TC, Yamaguchi H, Ruiz A, Martínez A, Madrigal L, Hincapié L, Arango JC, Anthony DC, Koo EH, Goate AM, Selkoe DJ, Arango JC (1996) The E280A presenilin 1 Alzheimer mutation produces increased A beta 42 deposition and severe cerebellar pathology. *Nat Med* **2**, 1146-1150.
- [5] Duque-Castaño A, Roldán MI, Arango-Viana JC, Arcos-Burgos M, Cubillo H, Lopera F (1999) Neuropathological

- findings in early-onset Alzheimer's disease (E280a-PS1 mutation). *Rev Neurol* **29**, 1-6.
- [6] Velez-Pardo C, Arellano JI, Cardona-Gomez P, Jimenez Del Rio M, Lopera F, De Felipe J (2004) CA1 hippocampal neuronal loss in familial Alzheimer's disease presenilin-1 E280A mutation is related to epilepsy. *Epilepsia* **45**, 751-756.
- [7] Quiroz YT, Sperling RA, Norton DJ, Baena A, Arboleda-Velasquez JF, Cosio D, Schultz A, Lapoint M, Guzman-Velez E, Miller JB, Kim LA, Chen K, Tariot PN, Lopera F, Reiman EM, Johnson KA (2018) Association between amyloid and tau accumulation in young adults with autosomal dominant Alzheimer disease. *JAMA Neurol* **75**, 548-556.
- [8] Palmqvist S, Janelidze S, Quiroz YT, Zetterberg H, Lopera F, Stomrud E, Su Y, Chen Y, Serrano GE, Leuzy A, Mattsson-Carlgen N, Strandberg O, Smith R, Villegas A, Sepulveda-Falla D, Chai X, Proctor NK, Beach TG, Blennow K, Dage JL, Reiman EM, Hansson O (2020) Discriminative accuracy of plasma phospho-tau217 for Alzheimer disease vs other neurodegenerative disorders. *JAMA* **324**, 772-781.
- [9] Dinkel F, Trujillo-Rodriguez D, Villegas A, Streffer J, Mercken M, Lopera F, Glatzel M, Sepulveda-Falla D (2020) Decreased deposition of beta-amyloid 1-38 and increased deposition of beta-amyloid 1-42 in brain tissue of presenilin-1 E280A familial Alzheimer's disease patients. *Front Aging Neurosci* **12**, 220.
- [10] Ghisays V, Lopera F, Goradia DD, Protas HD, Malek-Ahmadi MH, Chen Y, Devadas V, Luo J, Lee W, Baena A, Bocanegra Y, Guzmán-Vélez E, Pardilla-Delgado E, Vila-Castelar C, Fox-Fuller JT, Hu N, Clayton D, Thomas RG, Alvarez S, Espinosa A, Acosta-Baena N, Giraldo MM, Rios-Romenets S, Langbaum JB, Chen K, Su Y, Tariot PN, Quiroz YT, Reiman EM; API ADAD Colombia Trial Group (2021) PET evidence of preclinical cerebellar amyloid plaque deposition in autosomal dominant Alzheimer's disease-causing Presenilin-1 E280A mutation carriers. *Neuroimage Clin* **31**, 102749.
- [11] Tariot PN, Lopera F, Langbaum JB, Thomas RG, Hendrix S, Schneider LS, Rios-Romenets S, Giraldo M, Acosta N, Tobon C, Ramos C, Espinosa A, Cho W, Ward M, Clayton D, Friesenhahn M, Mackey H, Honigberg L, Sanabria Bohorquez S, Chen K, Walsh T, Langlois C, Reiman EM (2018) The Alzheimer's Prevention Initiative Autosomal-Dominant Alzheimer's Disease Trial: A study of crenezumab versus placebo in preclinical PSEN1 E280A mutation carriers to evaluate efficacy and safety in the treatment of autosomal-dominant Alzheimer's disease, including a placebo-treated noncarrier cohort. *Alzheimers Dement (N Y)* **4**, 150-160.
- [12] Dominici M, Le Blanc K, Mueller I, Slaper-Cortenbach I, Marini F, Krause D, Deans R, Keating A, Prockop Dj, Horwitz E (2006) Minimal criteria for defining multipotent mesenchymal stromal cells. The International Society for Cellular Therapy position statement. *Cytotherapy* **8**, 315-317.
- [13] Viswanathan S, Shi Y, Galipeau J, Krampera M, Leblanc K, Martin I, Nolte J, Phinney DG, Sensebe L (2019) Mesenchymal stem versus stromal cells: International Society for Cell & Gene Therapy (ISCT[®]) Mesenchymal Stromal Cell committee position statement on nomenclature. *Cytotherapy* **21**, 1019-1024.
- [14] Shariati A, Nemati R, Sadeghipour Y, Yaghoubi Y, Baghbani R, Javidi K, Zamani M, Hassanzadeh A (2020) Mesenchymal stromal cells (MSCs) for neurodegenerative disease: A promising frontier. *Eur J Cell Biol* **99**, 151097.
- [15] Choudhary P, Gupta A, Singh S (2021) Therapeutic advancement in neuronal transdifferentiation of mesenchymal stromal cells for neurological disorders. *J Mol Neurosci* **71**, 889-901.
- [16] Lv H, Hu Y, Cui Z, Jia H (2018) Human menstrual blood: A renewable and sustainable source of stem cells for regenerative medicine. *Stem Cell Res Ther* **9**, 325.
- [17] Chen L, Qu J, Cheng T, Chen X, Xiang C (2019) Menstrual blood-derived stem cells: Toward therapeutic mechanisms, novel strategies, and future perspectives in the treatment of diseases. *Stem Cell Res Ther* **10**, 406.
- [18] Liu Y, Niu R, Yang F, Yan Y, Liang S, Sun Y, Shen P, Lin J (2018) Biological characteristics of human menstrual blood-derived endometrial stem cells. *J Cell Mol Med* **22**, 1627-1639.
- [19] Zhao Y, Chen X, Wu Y, Wang Y, Li Y, Xiang C (2018) Transplantation of human menstrual blood-derived mesenchymal stem cells alleviates Alzheimer's disease-like pathology in APP/PS1 transgenic mice. *Front Mol Neurosci* **11**, 140.
- [20] Quintero-Espinosa D, Soto-Mercado V, Quintero-Quinchia C, Mendivil-Perez M, Velez-Pardo C, Jimenez-Del-Rio M (2021) Latent tri-lineage potential of human menstrual blood-derived mesenchymal stromal cells revealed by specific *in vitro* culture conditions. *Mol Neurobiol* **58**, 5194-5209.
- [21] Bonilla-Porras AR, Velez-Pardo C, Jimenez-Del-Rio M (2017) Fast transdifferentiation of human Wharton's jelly mesenchymal stem cells into neurospheres and nerve-like cells. *J Neurosci Methods* **282**, 52-60.
- [22] Soto-Mercado V, Mendivil-Perez M, Velez-Pardo C, Lopera F, Jimenez-Del-Rio M (2020) Cholinergic-like neurons carrying PSEN1 E280A mutation from familial Alzheimer's disease reveal intraneuronal sAPP β fragments accumulation, hyperphosphorylation of tau, oxidative stress, apoptosis and Ca²⁺ dysregulation: Therapeutic implications. *PLoS One* **15**, e0221669.
- [23] Soto-Mercado V, Mendivil-Perez M, Velez-Pardo C, Jimenez-Del-Rio M (2021) (-)-Epigallocatechin-3-gallate diminishes intra-and extracellular amyloid-induced cytotoxic effects on cholinergic-like neurons from familial Alzheimer's disease PSEN1 E280A. *Biomolecules* **11**, 1845.
- [24] Zarezaeh M, Barzegari M, Aghapour B, Adeli S, Khademi F, Musazadeh V, Jamilian P, Jamilian P, Fakhr L, Chehregosha F, Ghoreishi Z, Ostadrahimi A (2022) Melatonin effectiveness in amelioration of oxidative stress and strengthening of antioxidant defense system: Findings from a systematic review and dose-response meta-analysis of controlled clinical trials. *Clin Nutr ESPEN* **48**, 109-120.
- [25] Feng Z, Qin C, Chang Y, Zhang JT (2006) Early melatonin supplementation alleviates oxidative stress in a transgenic mouse model of Alzheimer's disease. *Free Radic Biol Med* **40**, 101-109.
- [26] Li Y, Zhang J, Wan J, Liu A, Sun J (2020) Melatonin regulates A β production/clearance balance and A β neurotoxicity: A potential therapeutic molecule for Alzheimer's disease. *Biomed Pharmacother* **132**, 110887.
- [27] Dai Y, Peng L, Liu Y, Xu Y, Qiao J (2021) Melatonin binds with high affinity and specificity to beta-amyloid: LC-MS provides insight into Alzheimer's disease treatment. *FEBS Open Bio* **11**, 2800-2806.

- [28] Zhu L, Gong Y, Lju H, Sun G, Zhang Q, Qian Z (2021) Mechanisms of melatonin binding and destabilizing the protofilament and filament of tau R3-R4 domains revealed by molecular dynamics simulation. *Phys Chem Chem Phys* **23**, 20615-20626.
- [29] Wang CF, Song CY, Wang X, Huang LY, Ding M, Yang H, Wang P, Xu LL, Xie ZH, Bi JZ (2019) Protective effects of melatonin on mitochondrial biogenesis and mitochondrial structure and function in the HEK293-APPswe cell model of Alzheimer's disease. *Eur Rev Med Pharmacol Sci* **23**, 3542-3550.
- [30] Roy J, Wong KY, Aquili L, Uddin MS, Heng BC, Tipoe GL, Wong KH, Fung ML, Lim LW (2022) Role of melatonin in Alzheimer's disease: From preclinical studies to novel melatonin-based therapies. *Front Neuroendocrinol* **65**, 100986.
- [31] Velez-Pardo C, Lopera F, Jimenez Del Rio M (2000) DNA damage does not correlate with amyloid-beta-plaques and neurofibrillary tangles in familial Alzheimer's disease presenilin-1 [E280A] mutation. *J Alzheimers Dis* **2**, 47-57.
- [32] Kaminska A, Wedzinska A, Kot M, Sarnowska A (2021) Effect of long-term 3D spheroid culture on WJ-MSC. *Cells* **10**, 719.
- [33] Bravo K, Alzate F, Osorio E (2016) Fruits of selected wild and cultivated Andean plants as sources of potential compounds with antioxidant and anti-aging activity. *Ind Crops Prod* **85**, 341-352.
- [34] Pap P, Koszeghy A, Szucs G, Rusznák Z (2009) Cytoplasmic Ca(2+) concentration changes evoked by cholinergic stimulation in primary astrocyte cultures prepared from the rat cochlear nucleus. *Hear Res* **255**, 73-83.
- [35] Schindelin J, Arganda-Carreras I, Frise E, Kaynig V, Longair M, Pietzsch T, Preibisch S, Rueden C, Saalfeld S, Schmid B, Tinevez JY, White DJ, Hartenstein V, Eliceiri K, Tomancak P, Cardona A (2012) Fiji: An open-source platform for biological-image analysis. *Nat Methods* **9**, 676-682.
- [36] Lasic SE, Clarke-Williams CJ, Munafò MR (2018) What exactly is 'N' in cell culture and animal experiments? *PLoS Biol* **16**, e2005282.
- [37] Bloom GS (2014) Amyloid-beta and tau: The trigger and bullet in Alzheimer disease pathogenesis. *JAMA Neurol* **71**, 505-508.
- [38] Wu HY, Kuo PC, Wang YT, Lin HT, Roe AD, Wang BY, Han CL, Hyman BT, Chen YJ, Tai HC (2018) β -amyloid induces pathology-related patterns of tau hyperphosphorylation at synaptic terminals. *J Neuropathol Exp Neurol* **77**, 814-826.
- [39] Mendivil-Perez M, Soto-Mercado V, Guerra-Librero A, Fernandez-Gil BI, Florido J, Shen YQ, Tējada MA, Capilla-Gonzalez V, Rusanova I, Garcia-Verdugo JM, Acuña-Castroviejo D, López LC, Velez-Pardo C, Jimenez-Del-Rio M, Ferrer JM, Escames G (2017) Melatonin enhances neural stem cell differentiation and engraftment by increasing mitochondrial function. *J Pineal Res* **63**, e12415.
- [40] da Silva Siqueira L, Majolo F, da Silva APB, da Costa JC, Marinovic DR (2021) Neurospheres: A potential *in vitro* model for the study of central nervous system disorders. *Mol Biol Rep* **48**, 3649-3663.
- [41] Ha J, Kang JS, Lee M, Baek A, Kim S, Chung SK, Lee MO, Kim J (2020) Simplified brain organoids for rapid and robust modeling of brain disease. *Front Cell Dev Biol* **8**, 594090.
- [42] Ochiishi T, Kaku M, Kiyosue K, Doi M, Urabe T, Hattori N, Shimura H, Ebihara T (2019) New Alzheimer's disease model mouse specialized for analyzing the function and toxicity of intraneuronal Amyloid β oligomers. *Sci Rep* **9**, 17368.
- [43] Okazawa H (2021) Intracellular amyloid hypothesis for ultra-early phase pathology of Alzheimer's disease. *Neuropathology* **41**, 93-98.
- [44] Welikovitsh LA, Do Carmo S, Maglóczy Z, Szocsics P, Lőke J, Freund T, Cuello AC (2018) Evidence of intraneuronal Abeta accumulation preceding tau pathology in the entorhinal cortex. *Acta Neuropathol* **136**, 901-917.
- [45] Gallego Villarejo L, Bachmann L, Marks D, Brachthäuser M, Geidies A, Müller T (2022) Role of intracellular amyloid β as pathway modulator, biomarker, and therapy target. *Int J Mol Sci* **23**, 4656.
- [46] Antonino M, Marmo P, Freitas CL, Quassollo GE, Sánchez MF, Lorenzo A, Bignante EA (2022) A β assemblies promote amyloidogenic processing of APP and intracellular accumulation of A β 42 through Go/G β γ signaling. *Front Cell Dev Biol* **10**, 852738.
- [47] Hilt S, Altman R, Kálai T, Maezawa I, Gong Q, Wachsmann-Hogiu S, Jin LW, Voss JC (2018) A bifunctional anti-amyloid blocks oxidative stress and the accumulation of intraneuronal amyloid-beta. *Molecules* **23**, 2010.
- [48] Schubert D, Kepchia D, Liang Z, Dargusch R, Goldberg J, Maher P (2019) Efficacy of cannabinoids in a pre-clinical drug-screening platform for Alzheimer's disease. *Mol Neurobiol* **56**, 7719-7730.
- [49] Soto-Mercado V, Mendivil-Perez M, Jimenez-Del-Rio M, Velez-Pardo C (2021) Multi-target effects of the cannabinoid CP55940 on familial Alzheimer's disease PSEN1 E280A cholinergic-like neurons: Role of CB1 receptor. *J Alzheimers Dis* **82**, S359-S378.
- [50] Tang G, Xu Y, Zhang C, Wang N, Li H, Feng Y (2021) Green tea and epigallocatechin gallate (EGCG) for the management of nonalcoholic fatty liver diseases (NAFLD): Insights into the role of oxidative stress and antioxidant mechanism. *Antioxidants (Basel)* **10**, 1076.
- [51] Andrich K, Bieschke J (2015) The effect of (-)-Epigallo-catechin-(3)-gallate on amyloidogenic proteins suggests a common mechanism. *Adv Exp Med Biol* **863**, 139-161.
- [52] Sonawane SK, Chidambaram H, Boral D, Gorantla NV, Balmik AA, Dangi A, Ramasamy S, Marelli UK, Chinnathambi S (2020) EGCG impedes human tau aggregation and interacts with tau. *Sci Rep* **10**, 12579.
- [53] Reiter RJ, Melchiorri D, Sewerynek E, Poeggeler B, Barlow-Walden L, Chuang J, Ortiz GG, Acuña-Castroviejo D (1995) A review of the evidence supporting melatonin's role as an antioxidant. *J Pineal Res* **18**, 1-11.
- [54] Pappolla M, Bozner P, Soto C, Shao H, Robakis NK, Zagorski M, Frangione B, Ghiso J (1998) Inhibition of Alzheimer beta-fibrillogenesis by melatonin. *J Biol Chem* **273**, 7185-7188.
- [55] Ali T, Kim MO (2015) Melatonin ameliorates amyloid beta-induced memory deficits, tau hyperphosphorylation and neurodegeneration via PI3/Akt/GSk3 β pathway in the mouse hippocampus. *J Pineal Res* **59**, 47-59.
- [56] Chen D, Zhang T, Lee TH (2020) Cellular mechanisms of melatonin: Insight from neurodegenerative diseases. *Biomolecules* **10**, 1158.
- [57] Reiter RJ, Rosales-Corral S, Tan DX, Jou MJ, Galano A, Xu B (2017) Melatonin as a mitochondria-targeted antioxidant: One of evolution's best ideas. *Cell Mol Life Sci* **74**, 3863-3881.

- [58] Jang MH, Jung SB, Lee MH, Kim CJ, Oh YT, Kang I, Kim J, Kim EH (2005) Melatonin attenuates amyloid beta₂₅₋₃₅-induced apoptosis in mouse microglial BV2 cells. *Neurosci Lett* **380**, 26-31.
- [59] Su-Hyun, J, Seung-Hyun, L, Kyong-Tai K, Se-Young C (2019) Melatonin inhibits nicotinic acetylcholine receptor functions in bovine chromaffin cells. *Int J Oral Biol* **44**, 50-54.
- [60] Ayar A, Martin DJ, Ozcan M, Kelestimur H (2001) Melatonin inhibits high voltage activated calcium currents in cultured rat dorsal root ganglion neurones. *Neurosci Lett* **313**, 73-77.
- [61] Singh NA, Mandal AK, Khan ZA (2016) Potential neuroprotective properties of epigallocatechin-3-gallate (EGCG). *Nutr J* **15**, 60.
- [62] Wang Y, Wang K, Yan J, Zhou Q, Wang X (2022) Recent progress in research on mechanisms of action of natural products against Alzheimer's disease: Dietary plant polyphenols. *Int J Mol Sci* **23**, 13886.
- [63] Henning SM, Fajardo-Lira C, Lee HW, Youssefian AA, Go VL, Heber D (2003) Catechin content of 18 teas and a green tea extract supplement correlates with the antioxidant capacity. *Nutr Cancer* **45**, 226-235.
- [64] Zhong Y, Ma CM, Shahidi F (2012) Antioxidant and antiviral activities of lipophilic epigallocatechin gallate (EGCG) derivatives. *J Funct Foods* **4**, 87-93.
- [65] Zhao C, Li C, Liu S, Yang L (2014) The galloyl catechins contributing to main antioxidant capacity of tea made from *Camellia sinensis* in China. *ScientificWorldJournal* **2014**, 863984.
- [66] Badmus JA, Ekpo OE, Rautenbach F, Marnewick JL, Hussein AA, Hiss DC (2016) Isolation and antioxidant activity of flavonoids from *Holarrhena floribunda* (G.don) leaves. *Acta Biochim Pol* **63**, 353-358.
- [67] Jiang C, Wang L, Huang X, Zhu S, Ma C, Wang H (2021) Structural characterization and antioxidant property of enzymatic-transesterification derivatives of (-)-epigallocatechin-3-O-gallate and vinyl laurate. *J Food Sci* **86**, 4717-4729.
- [68] Pieri C, Marra M, Moroni F, Recchioni R, Marcheselli F (1994) Melatonin: A peroxy radical scavenger more effective than vitamin E. *Life Sci* **55**, PL271-276.
- [69] Sofic E, Rimpapa Z, Kundurovic Z, Sapcanin A, Tahirovic I, Rustembegovic A, Cao G (2005) Antioxidant capacity of the neurohormone melatonin. *J Neural Transm (Vienna)* **112**, 349-358.
- [70] Fu Y, Chen Y, Jin Z, Gao H, Song G, Wang Q, Xu K (2022) Melatonin alleviates oxidative stress induced by H₂O₂ in porcine trophectoderm cells. *Antioxidants (Basel)* **11**, 1047.
- [71] Roell KR, Reif DM, Motsinger-Reif AA (2017) An introduction to terminology and methodology of chemical synergy-perspectives from across disciplines. *Front Pharmacol* **8**, 158.
- [72] Safwat MA, Kandil BA, Elblbesy MA, Soliman GM, Eleraky NE (2020) Epigallocatechin-3-gallate-loaded gold nanoparticles: Preparation and evaluation of anticancer efficacy in Ehrlich tumor-bearing mice. *Pharmaceuticals (Basel)* **13**, 254.
- [73] Chuffa LGA, Seiva FRF, Novais AA, Simão VA, Martín Giménez VM, Manucha W, Zuccari DAPC, Reiter RJ (2021) Melatonin-loaded nanocarriers: New horizons for therapeutic applications. *Molecules* **26**, 3562.